PHYSIOLOGY

Mechanical activation of TRPV4 channels controls albumin reabsorption by proximal tubule cells

Roberta Gualdani[1], François Seghers[1], Xavier Yerna[1], Olivier Schakman[1], Nicolas Tajeddine[1], Younès Achouri[2], Fadel Tissir[3], Olivier Devuyst[4], Philippe Gailly[1]*

Defects in protein reabsorption by the proximal tubule are toxic for epithelial cells in the nephron and may result in nephropathy. In this study, we showed that the ion channel TRPV4 modulated the endocytosis of albumin and low–molecular weight proteins in the proximal tubule. TRPV4 was found at the basolateral side of proximal tubule cells, and its mechanical activation by cell stretching induced Ca^{2+} entry into the cytosol, which promoted endocytosis. *Trpv4*$^{-/-}$ mice presented with mild proximal tubule dysfunction under basal conditions. To challenge endocytic function, the permeability of the glomerular filter was altered by systemic delivery of angiotensin II. The proteinuria induced by this treatment was more severe in *Trpv4*$^{-/-}$ than in *Trpv4*$^{+/+}$ mice. Injecting antibodies against the glomerular basement membrane to induce glomerulonephritis is a more pathophysiologically relevant method of impairing glomerular filter permeability. Albuminuria was more severe in mice that lacked TRPV4 specifically in the proximal tubule than in control mice. These results emphasize the importance of TRPV4 in sensing pressure in the proximal tubule in response to variations in the amount of ultrafiltrate and unveil a mechanism that controls protein reabsorption.

INTRODUCTION

The proximal tubule (PT) is the first segment of the kidney tubule, and it reabsorbs about 70% of the water, ions, and solutes filtrated by the glomerulus using transcellular and paracellular transports. The epithelial cells lining the PT express the multiligand receptors megalin [low-density lipoprotein–related protein 2 (LRP2)] and cubilin, which mediate the endocytosis of various substrates, among which are albumin and low–molecular weight proteins (LMWPs) (*1*–*4*). Albumin is reabsorbed through both megalin- and cubilin-mediated clathrin-coated pits into vesicles and by fluid-phase endocytosis. The progressive acidification of endosomes can induce dissociation of albumin from megalin and cubilin receptors and enhance its binding to the neonatal Fc receptor (FcRn). Albumin can thus be sorted either to a megalin- and cubilin-directed lysosomal degradation or to an FcRn-mediated transcytotic pathway, thereby allowing its recycling at the basolateral side and explaining its particular long half-life (19 days in humans) (*5*).

Urinary albumin and LMWPs are critical to disease progression. Renal tubules are vulnerable to proteinuria, and in response to injury, tubular epithelial cells undergo changes and function as inflammatory and fibrogenic cells. This process thus contributes to the progression of chronic kidney disease (*6*, *7*). Under physiological conditions, the filtration of albumin is greater than previously thought, which therefore emphasizes the role of PT in minimizing albuminuria through reabsorption of albumin (*4*, *8*).

Variations in the glomerular filtration rate (GFR) modulate PT function. Elevation of GFR increases Na^+ reabsorption by inducing the insertion of transporters into the apical membrane (*9*). Increased fluid flow may also modulate LMWP endocytosis, although this effect has been shown only in immortalized cultured PT cells [reviewed in (*10*)]. The modulation of PT function by the amount of ultrafiltrate delivered to the PT suggests the presence of mechanotransduction pathways. The ultrafiltrated volume propelled into the PT creates a flow at the apical surface of the PT and raises the intraluminal pressure at a mean of 10 to 15 mmHg (*11*), but the flow is pulsatile, with an amplitude and a frequency varying according to filtration pressure and heart rate. Two types of force are thus developed by the entry of the ultrafiltrate in the PT lumen: a shear stress on the apical membrane and a radial stretch as changes in intraluminal hydrostatic pressure modify the tubule diameter. Shear stress could be sensed by the primary cilium, at least in immortalized PT cells (*10*). Radial stretch is sensed by cytoskeleton, adhesion proteins, and/or stretch-sensitive ion channels at the basolateral or apical sides of the epithelial cells (*4*). The best candidate channels that could transduce mechanical inputs into ion currents under physiological conditions seem to be Piezo1, Piezo2, and Transient Receptor Potential channel subfamily V member 4 (TRPV4) channels (*12*). In PT cells, Piezo1 acts as a stretch-activated cationic channel, and polycystin-2 (PC2) inhibits its activity (*13*). The role of TRPV4 in the PT is so far unknown. TRPV4 is a polymodal ion channel (*14*) that responds to unrelated stimuli, including temperature, osmotic, and chemical stimulations (*15*–*19*). At the physiological level, TRPV4 plays a role in the mechanotransduction pathways of various cell types and tissues, including dorsal root ganglia (DRG) neurons (*20*), osteoblasts and osteoclasts (*21*, *22*), chondrocytes (*23*), and urothelium (*24*). TRPV4 is particularly enriched in the kidney, and TRPV4 participates in flow sensing in the collecting duct and MDCK kidney epithelial cells (*25*, *26*). We also showed that it constitutes the mechanosensor of the juxtaglomerular apparatus, triggering the inhibition of renin secretion when blood pressure increases (*27*). In the present paper, we report that TRPV4 was abundantly expressed at the basolateral side of PT cells and that its mechanical activation controlled receptor-mediated and fluid-phase endocytosis of albumin. In *Trpv4*$^{-/-}$ mice and in mice with PT-specific conditional deletion of *Trpv4*, mechanically induced endocytosis was altered.

[1]Université catholique de Louvain, Institute of Neuroscience, Cell Physiology, av. Mounier 53/B1.53.17, B-1200 Brussels, Belgium. [2]Université catholique de Louvain, de Duve Institute, Transgenic Core Facility, av. Hippocrate 75/B1.75.09, B-1200 Brussels, Belgium. [3]Université catholique de Louvain, Institute of Neuroscience, Developmental Neurobiology, av. Hippocrate 73/B1.73.16, B-1200 Brussels, Belgium. [4]University of Zurich, Institute of Physiology, Winterthurerstr. 190, CH-8057 Zurich, Switzerland.
*Corresponding author. Email: philippe.gailly@uclouvain.be

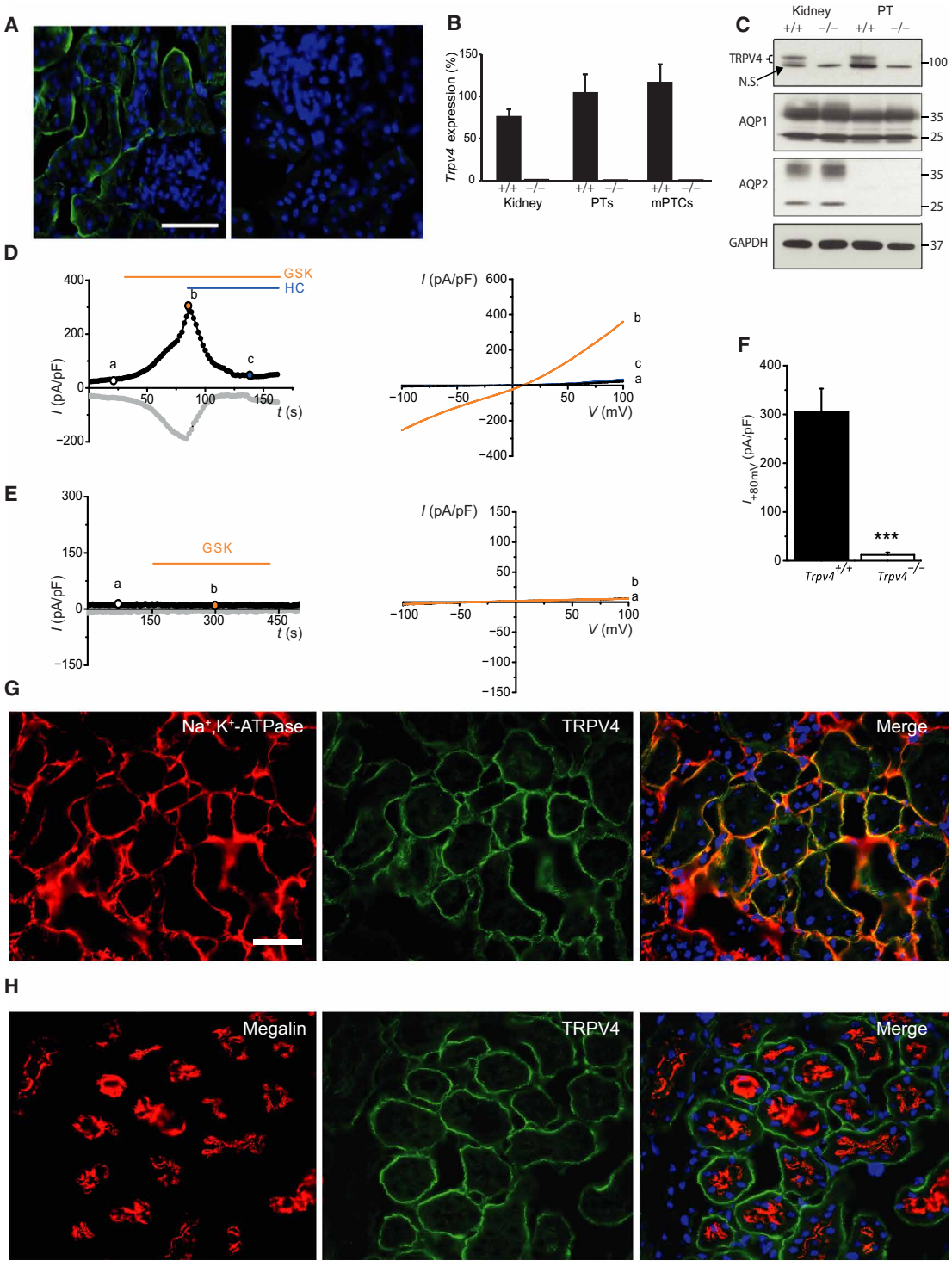

Fig. 1. TRPV4 is expressed and is functional in proximal tubule cells. (**A**) Immunolabeling of TRPV4 (in green) on renal cortex sections from *Trpv4*$^{+/+}$ (left) and *Trpv4*$^{-/-}$ mice (right). TRPV4 is mainly expressed at the basolateral side of PT epithelial cells. Nuclei are stained in blue with 4′,6-diamidino-2-phenylindole (DAPI; 1 μg/ml). Scale bar, 50 μm ($n = 3$ sections for each group). (**B**) Quantitative analysis of mRNA expression of *Trpv4* in kidneys, proximal tubules (PT), and primary cultured PT cells (mPTCs) isolated from *Trpv4*$^{+/+}$ and *Trpv4*$^{-/-}$ mice ($n = 5$ mice for each genotype). (**C**) Western blotting of total kidney extracts, PTs, and mPTCs from control (+/+) and knockout (−/−) mice ($n = 3$ mice for each genotype). In *Trpv4*$^{+/+}$ samples, in addition to the expected specific band at 107-kDa, a nonspecific band (N.S.) around 75 kDa is also detected, as mentioned in other publications using antibodies directed against the same epitope as used here [amino acids 853 to 871; see, for example, (*68*)]. Anti-AQP1 and anti-AQP2 antibodies were positive and negative markers of PTs, respectively. Anti–glyceraldehyde-3-phosphate dehydrogenase (GAPDH) was used as a loading control. (**D**) Left: Representative time courses of whole-cell currents recorded at +80 and −80 mV (black and gray curves, respectively) in *Trpv4*$^{+/+}$ mPTCs in the presence of 100 nM GSK1016790A and 1 μM HC067047 (HC) at the indicated time intervals. Right: Representative current/voltage (*I-V*) traces (from −100 to +100 mV repeated every 2 s) obtained at the time points indicated in (D). (**E**) Same as (D), except that mPTCs were isolated from *Trpv4*$^{-/-}$ mice. (**F**) Pooled data of whole-cell currents (at +80 mV) evoked by 100 nM GSK1016790A in mPTCs from *Trpv4*$^{+/+}$ and *Trpv4*$^{-/-}$mice ($n = 8$ cells for each genotype). ***$P < 0.001$ (unpaired Student's *t* test). (**G** and **H**) Coimmunolabeling of TRPV4 (in green) and Na^+/K^+-ATPase (G, red) or megalin (H, red) in renal cortex sections from *Trpv4*$^{+/+}$ mice ($n = 3$ sections for each condition). Scale bar, 50 μm. AQP1, aquaporin 1; AQP2, aquaporin 2.

RESULTS

TRPV4 is expressed and functional in PT cells

Immunolocalization demonstrated the presence of TRPV4 in PT cells, mainly at the basolateral membrane, as well as a smaller amount at the apical membranes (Fig. 1A). We generated *Trpv4*$^{-/-}$ mice (fig. S1) and studied the function of TRPV4 with cultured primary PT cells (mPTCs) from *Trpv4*$^{-/-}$ and *Trpv4*$^{+/+}$ mice (*28*). TRPV4 was expressed at the mRNA and protein levels in microdissected PTs

and mPTCs (Fig. 1, B and C). In patch-clamp recordings of mPTCs from *Trpv4*$^{+/+}$ mice, application of the TRPV4 agonist GSK1016790A [*N*-((1*S*)-1-{[4-((2*S*)-2-{[(2,4-dichlorophenyl)sulfonyl]amino}-3-hydroxypropanoyl)-1-piperazinyl]carbonyl}-3-methylbutyl)-1-benzothiophene-2-carboxamide] elicited an outwardly rectifying current, which was blocked by the TRPV4 antagonist HC067047 (Fig. 1D). No current was observed in response to GSK1016790A in mPTCs from *Trpv4*$^{-/-}$ mice (Fig. 1, E and F). No statistical difference was observed between the membrane capacitance of *Trpv4*$^{+/+}$ and *Trpv4*$^{-/-}$ mPTCs (fig. S2). Immunofluorescence staining of PTs showed that TRPV4 colocalized with the Na^+/K^+-ATPase (Fig. 1G), which is located within the basolateral membrane, and was distinctly distributed from megalin, a marker of the apical side of PT (Fig. 1H).

TRPV4 is a mechanosensor in mPTCs

We next investigated whether we could mechanically activate TRPV4 in mPTCs. Because TRPV4 has been described to be a flow sensor in the collecting duct (*29*), we first tested the response of mPTCs to shear stress. When flow was applied to the surface of the cells, some sparse responses were observed among mPTCs. However, this phenomenon was independent of TRPV4 expression (Fig. 2, A and B). The application of a hypotonic solution to induce cell swelling triggered a $[Ca^{2+}]_i$ transient in mPTCs that was absent in *Trpv4*$^{-/-}$ cells (Fig. 2, C and D). This finding suggested that TRPV4 could act as a stretch sensor in the PT. In mPTCs cultured on stretchable silicon chambers, stretching to induce substrate deformation induced a rise in $[Ca^{2+}]_i$. In *Trpv4*$^{-/-}$ cells, the response to stretch was significantly decreased in amplitude compared with wild-type cells (Fig. 2, E and F). Moreover, in the presence of the phospholipase A2 inhibitor 3-(4-octadecylbenzoyl)acrylic acid (OBAA), the amplitude of Ca^{2+} transient was not reduced (fig. S3). Last, we observed that this response depended on the presence of extracellular Ca^{2+}, suggesting the requirement for Ca^{2+} entry through a mechanically activated channel (Fig. 2G).

TRPV4 is an osmosensor in mPTCs

TRPV4 was originally identified as a channel activated by hypotonic cell swelling (*19*, *30*–*32*). Patch-clamp recordings revealed robust current activation in response to hypotonic shock not only in *Trpv4*$^{+/+}$ mPTCs (Fig. 3A) but also in *Trpv4*$^{-/-}$ mPTCs (Fig. 3B). This current

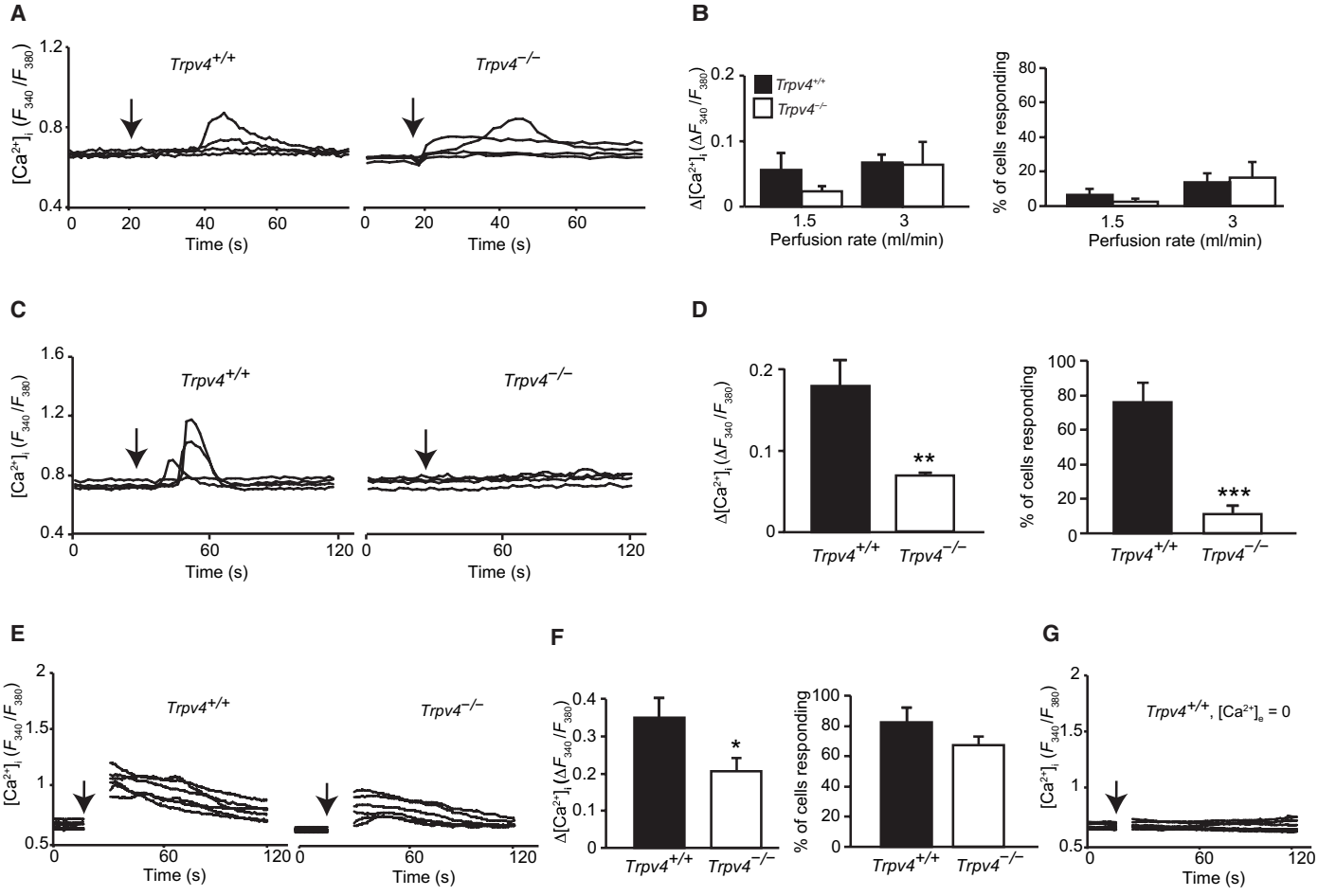

Fig. 2. Mechanical response of mPTCs. (**A** to **G**) Changes in $[Ca^{2+}]_i$ were assessed during flow stimulation (A and B), hypotonic cell swelling (C and D), and cell stretching (E and F). For each stimulus, representative curves of individual mPTCs are shown for *Trpv4*$^{+/+}$ and *Trpv4*$^{-/-}$ cells (A, C, and E). In (G), representative curves of individual *Trpv4*$^{+/+}$ mPTCs stretched in the absence of extracellular Ca^{2+} (*Trpv4*$^{+/+}$, $[Ca^{2+}]_e = 0$) are shown. Average increase in $[Ca^{2+}]_i$ and proportion of responding cells upon flow stimulation, hypotonic cell swelling, and cell stretching (B, D, and F) ($n = 5$ experiments with 15 to 20 cells per experiment and for each genotype). *$P < 0.05$, **$P < 0.01$, and ***$P < 0.001$ compared with *Trpv4*$^{+/+}$ cells (unpaired Student's *t* test).

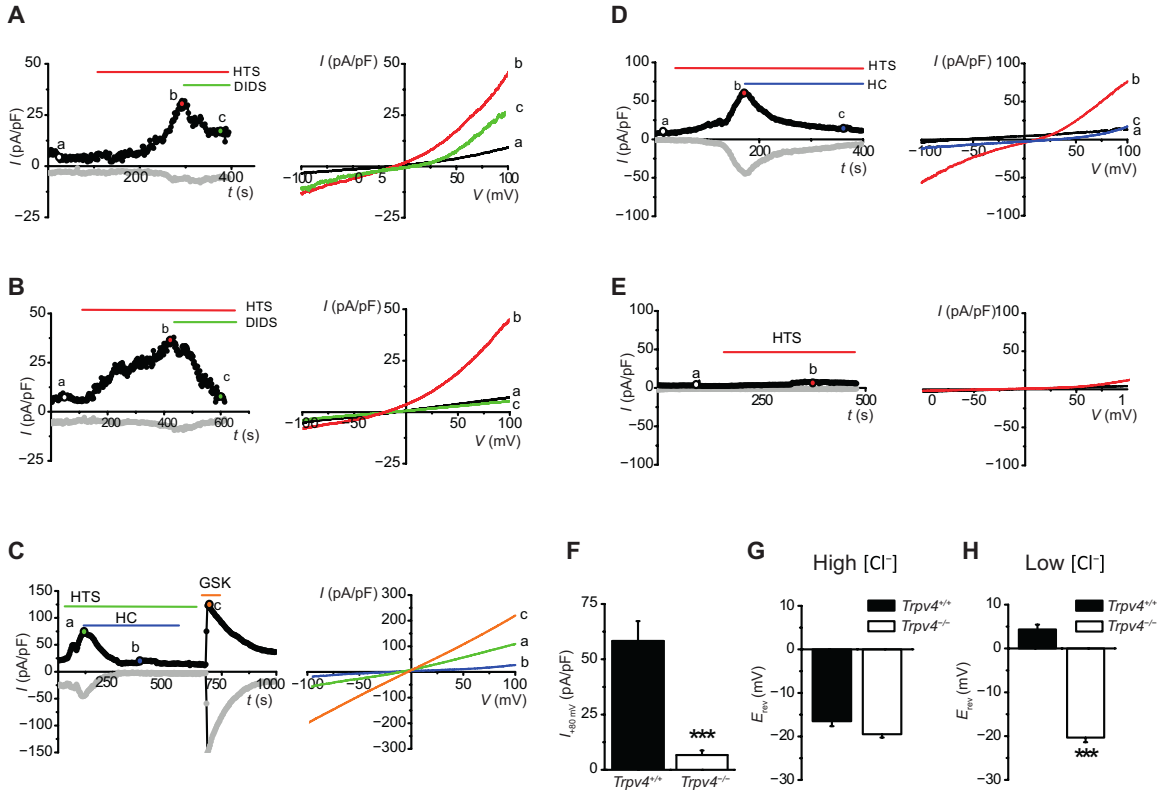

Fig. 3. Hypotonic swelling–induced activation of TRPV4 in mPTCs. (**A**) Representative time courses (left) recorded at +80 and −80 mV (black and gray curves, respectively) and *I-V* traces (right) of whole-cell currents in *Trpv4*$^{+/+}$ mPTCs in the presence of high Cl^- containing hypotonic solution (HTS) and DIDS (100 μM) at the indicated time intervals ($n = 6$ cells). (**B**) Representative time courses (left) recorded at +80 and −80 mV (black and gray curves, respectively) and *I-V* traces (right) of whole-cell currents in *Trpv4*$^{-/-}$ mPTCs in the presence of high Cl^-–containing hypotonic solution (HTS) and DIDS (100 μM) at the indicated time intervals ($n = 6$ cells). (**C**) Representative time courses (left) and *I-V* traces (right) of whole-cell current from *Trpv4*$^{+/+}$ mPTCs in the presence of low Cl^- hypotonic solution and HC067047 (1 μM) at the indicated time intervals ($n = 6$ cells). (**D**) Representative time courses (left) and *I-V* traces (right) of whole-cell current from *Trpv4*$^{-/-}$ mPTCs in the presence of low Cl^- hypotonic solution and HC067047 (1 μM) at the indicated time intervals ($n = 6$ cells). (**E**) Representative time courses (left) recorded at +80 and − 80 mV (black and gray curves, respectively) and *I-V* traces (right) of whole-cell currents from *Trpv4*$^{+/+}$ mPTCs in the presence of hypotonic solution, HC067047 (1 μM) and GSK1016790A (100 nM) at the indicated time intervals, in the continuous presence of DIDS (100 μM; $n = 6$ cells). (**F**) Pooled data of whole-cell currents (at +80 mV) evoked by low Cl^-–containing hypotonic solution from mPTCs isolated from *Trpv4*$^{+/+}$ and *Trpv4*$^{-/-}$ mice ($n = 6$ cells for each group). ***$P < 0.001$ (unpaired Student's *t* test). (**G**) Summary of E_{rev} recordings obtained from all *I-V* curves in *Trpv4*$^{+/+}$ and *Trpv4*$^{-/-}$ mPTCs during administration of high Cl^- hypotonic solution ($n = 6$ cells, not significant; unpaired Student's *t* test). (**H**) Summary of E_{rev} recordings obtained from all *I-V* curves in *Trpv4*$^{+/+}$ and *Trpv4*$^{-/-}$ mPTCs during administration of low Cl^- hypotonic solution ($n = 6$ cells). ***$P < 0.001$; unpaired Student's *t* test.

had the properties originally described for $I_{Cl,swell}$ (*33*, *34*), in that it had a reversal potential close to the predicted Cl^- equilibrium potential (~ −20 mV), it was outwardly rectified, and it was reverted in the presence of a high concentration of the Cl^- channel blocker DIDS (4,4′-diisothiocyano-2,2′-stilbenedisulfonic acid). DIDS partially blocked the current elicited by hypotonic cell swelling in *Trpv4*$^{+/+}$ mPTCs (Fig. 3A), but completely blocked this current in *Trpv4*$^{-/-}$ mPTCs (Fig. 3B). In *Trpv4*$^{+/+}$ mPTCs, the residual current remaining after application of DIDS showed a reversal potential close to 0 mV, suggesting a different ion selectivity, compared to the unblocked current (Fig. 3A). To test whether DIDS impaired the functionality of TRPV4 channel, we perfused *Trpv4*$^{+/+}$ mPTCs with a DIDS-containing hypotonic solution, which activated an outwardly rectifying current with a reversal potential of ~0 mV that was blocked by the TRPV4 antagonist HC067047 (Fig. 3C). The response to GSK1016790A was not inhibited by DIDS. Our data suggested that the residual current after pharmacological block of Cl^- conductance in response to hypotonic shock in *Trpv4*$^{+/+}$ mPTCs was due to TRPV4 activation. A low Cl^- hypotonic solution evoked an outwardly rectifying current that was blocked by HC067047 (Fig. 3D) and that was significantly smaller in *Trpv4*$^{-/-}$ mPTCs (Fig. 3, E and F), suggesting that TRPV4 contributes to the current rise elicited by hypotonic shock in PT. The reversal potential of the current elicited by a low Cl^- hypotonic solution was ~5 mV, whereas the reversal potential of the current activated in response to a high Cl^- hypotonic shock was ~−20 mV (Fig. 3, G and H), suggesting differences in ion permeability.

Stretch-activated channel activity in mPTCs

To investigate the role of TRPV4 in the mechanosensitivity of the PT, we performed high-speed pressure-clamp experiments on mPTCs. Stretch-activated channel (SAC) activity was elicited by negative suction pulses of 500 ms, and patch-clamp recordings were performed in cell-attached configuration at holding potential of −80 mV. As described previously (*13*), currents were characterized by a fast activation, lack of inactivation, and a slow deactivation at the end of the pressure pulse (Fig. 4A). Our data showed that membrane stretch–induced currents had similar amplitude and kinetics in *Trpv4*$^{+/+}$ and *Trpv4*$^{-/-}$ mPTCs (Fig. 4, A and B). Moreover, we

tested the response of SACs in the presence of GsMTx-4, the only drug known to specifically inhibit cationic SACs without inhibiting other ion channel families, such as voltage-gated K^+ and Ca^{2+} channels (*35*, *36*). SAC currents were blocked by extracellular GsMTx-4 [Fig. 4, A (bottom) and C]. Last, we showed that HC067047 did not affect SAC currents in *Trpv4*$^{+/+}$ cells (Fig. 4C). These results show that mPTCs do express channels other than TRPV4 that respond to fast membrane stretching. The GsMTx-4–inhibitable currents observed are similar to those described by Peyronnet *et al.* (*13*), who attributed them to Piezo1 channels based on targeted siRNA data.

TRPV4 channel activation triggers albumin endocytosis in mPTCs

Considering the results above suggesting that PT epithelial cells responded to mechanical cell stretch and because PT functions are controlled by the amount of ultrafiltrate delivered to the PT, we next investigated the possible role of TRPV4 in endocytosis in the PT. mPTCs were cultured on collagen-coated membranes, allowing them to keep a high degree of differentiation and a high endocytic uptake capacity (*37*, *38*), and exposed to fluorescein isothiocyanate (FITC)–albumin to enable tracking of receptor-mediated endocytosis. Endocytic uptake of albumin after pharmacological activation of TRPV4 with GSK1016790A was significantly higher in *Trpv4*$^{+/+}$ cells compared with the basal level, an effect not observed in *Trpv4*$^{-/-}$ cells (Fig. 5A). The uptake process of receptor-mediated endocytosis is characterized by saturation kinetics (*37*). As expected, uptake of FITC-albumin at 37°C saturated as a function of dose (Fig. 5B). In *Trpv4*$^{+/+}$ cells, activation of TRPV4 with GSK1016790A increased the V_{max} value without significantly changing the K_m value (V_{max} and K_m values were extrapolated using Michaelis-Menten kinetics; table S1), an effect not observed in *Trpv4*$^{-/-}$ cells. Moreover, the ability of GSK1016790A to increase V_{max} values was abolished in the absence of extracellular Ca^{2+}, indicating that Ca^{2+} influx across the plasma membrane was required for increasing endocytosis (Fig. 5C). Last, stretching the cells increased albumin uptake, and this effect was reduced by more than two-thirds in *Trpv4*$^{-/-}$ cells and when TRPV4 was blocked by HC067047 (Fig. 5, D and E). Residual stretch-dependent uptake of albumin observed in *Trpv4*$^{-/-}$ cells and after inhibition by HC06047 might be due to another mechanosensitive channel such as Piezo1 mentioned above. FITC-albumin uptaken after TRPV4 activation transited through the endolysosomal pathway as demonstrated by the substantial colocalization of FITC-albumin–positive vesicles with the endosome marker Ras-related protein 7 (Rab-7) and the lysosome marker LAMP1 (lysosomal-associated membrane protein 1), after treatment with GSK1016790A (Fig. 5, F and G). Fluid-phase endocytosis as evaluated by the uptake of FITC-labeled 70-kDa dextran was also enhanced by pharmacological activation of TRPV4, an effect that was significantly reduced in *Trpv4*$^{-/-}$ PT cells (fig. S4).

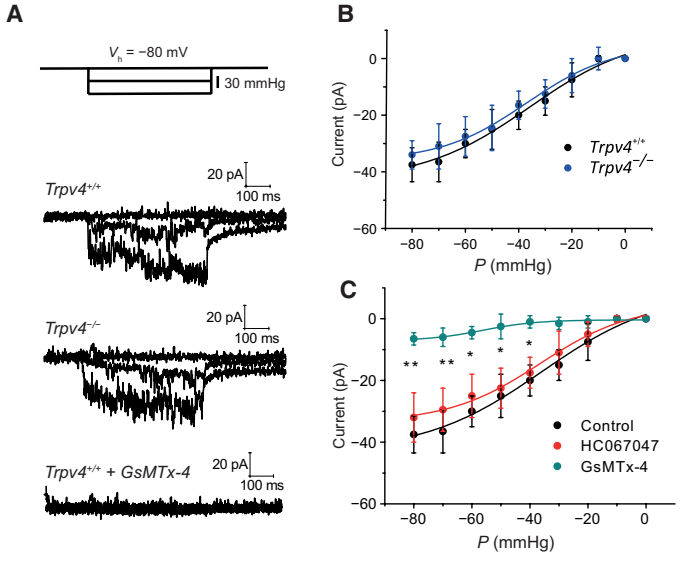

Fig. 4. Stretch-activated channel activity in mPTCs. (**A**) Cell-attached patch-clamp recording of stretch-activated channel (SAC) activity in mPTCs isolated from *Trpv4*$^{+/+}$ and *Trpv4*$^{-/-}$ mice in the presence or in the absence of GsMTx-4 (10 μM) at a holding potential of −80 mV. Top trace illustrates the pressure pulse protocol. (**B**) Normalized current-pressure relationships of SACs in mPTCs from *Trpv4*$^{+/+}$ and *Trpv4*$^{-/-}$ mice at a holding potential of −80 mV, fitted with a Boltzmann equation ($n = 8$ cells). The P_{50} values extrapolated from the fitting are the following: −35.8 ± 4.6 mmHg (*Trpv4*$^{+/+}$) and −38.9 ± 3.7 mmHg (*Trpv4*$^{-/-}$). (**C**) Normalized current-pressure relationships of SACs in mPTCs from *Trpv4*$^{+/+}$ mice in the presence of HC067047 (1 μM) and GsMTx-4 (10 μM). Results are shown as means ± SEM ($n = 8$ cells for each condition). The P_{50} values extrapolated from the fitting are the following: −36.4 ± 2.7 mmHg (HC067047) and −56.4 ± 4.1 mmHg [GsMTx-4; $^*P < 0.05$ and $^{**}P < 0.01$, two-way analysis of variance (ANOVA) test].

TRPV4 plays a role in tubular proteinuria

Using *Trpv4*$^{-/-}$ mice generated by Liedtke and Friedman (*39*), we previously reported that no major PT dysfunction is evident in *Trpv4*$^{-/-}$ mice under basal conditions (*40*), in particular glycosuria, phosphaturia, or proteinuria. In the *Trpv4*$^{-/-}$ mouse model developed here, we confirmed these results but found a significantly higher urinary concentration of CC16, a protein secreted by bronchial Clara cells and reabsorbed exclusively by receptor-mediated endocytosis in the early segments of the PT (Fig. 6A) (*41*). The higher concentration of CC16 observed in *Trpv4*$^{-/-}$ mouse in the absence of a frank albuminuria suggested mild PT dysfunction. We hypothesized that TRPV4 could be activated during PT mechanical loading, which would be expected to trigger processes that increase reabsorptive activity. To increase the luminal protein delivery to the PT to challenge its endocytic capacity, we used a protocol consisting of continuously delivering angiotensin II (AT2) using osmotic minipumps to increase the permeability of the glomerular filter (*42*). Diuresis was significantly increased upon AT2 infusion in both *Trpv4*$^{-/-}$ and control mice (Fig. 6B). Creatinine clearance was similarly altered by AT2 treatment (fig. S5), indicating a similar impairment of the glomerular filtration. AT2 increased albuminuria in control mice, but this increase was much larger in *Trpv4*$^{-/-}$ mice (Fig. 6C). Because TRPV4 is not expressed in the glomerulus and because the diuresis and the GFR were affected to similar extents in AT2-treated *Trpv4*$^{-/-}$ and *Trpv4*$^{+/+}$ mice, the specific increase in proteinuria observed in *Trpv4*$^{-/-}$ mice is suggestive of an endocytosis defect in *Trpv4*$^{-/-}$ PT (*4*). Moreover, no significant differences in phosphate and glucose urinary levels were found between the two genotypes during the AT2 infusion, suggesting a specific effect on endocytosis (Fig 6, D and E). Gene expression analysis suggested that the higher proteinuria observed in *Trpv4*$^{-/-}$ mice after AT2 injection was not attributable to down-regulation of genes encoding megalin, cubulin, rabankyrin, KIM-1, Dab-2, and Rab-5, factors typically involved in endocytosis (fig. S6) (*3*).

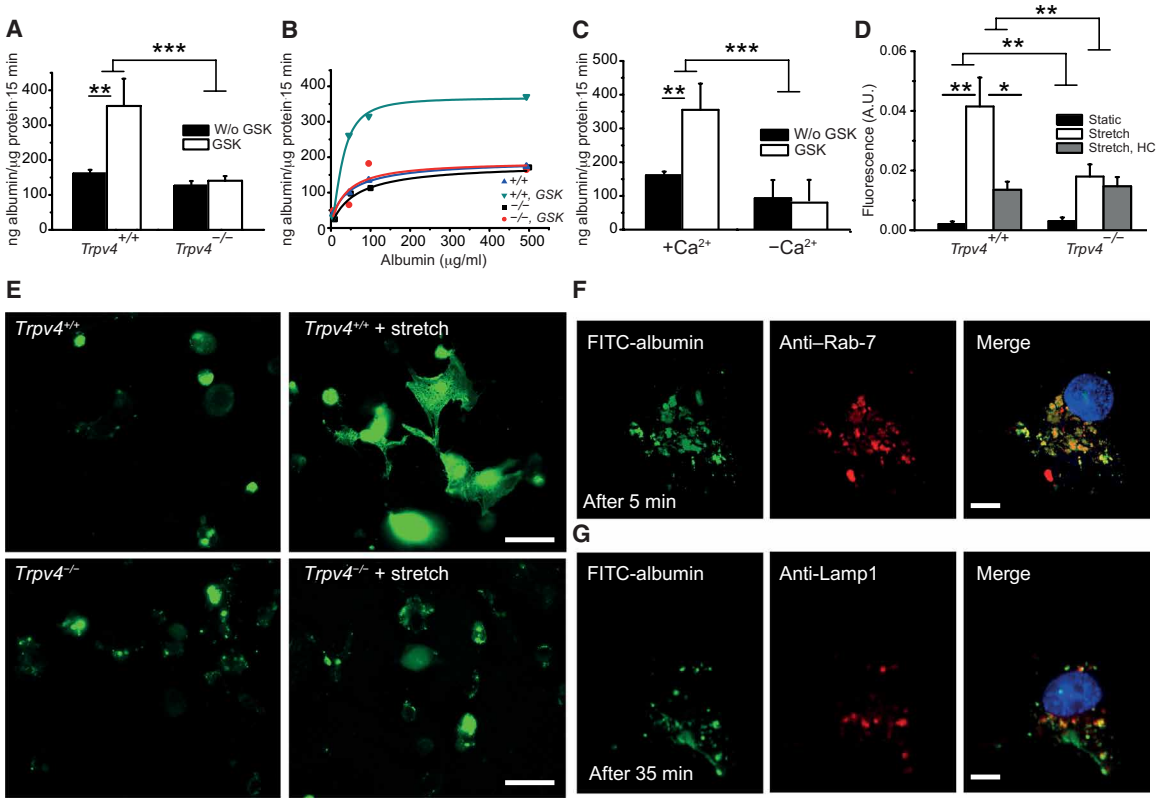

Fig. 5. TRPV4 promotes endocytosis in mPTCs in vitro. (**A**) Quantification of the total albumin uptake in *Trpv4*$^{+/+}$ and *Trpv4*$^{-/-}$ mPTCs seeded on collagen-coated membranes after incubation with FITC-albumin (0.5 mg/ml) for 15 min, in the absence or in the presence of 100 nM GSK1016790A. The fluorescence was normalized to the total lysed protein ($n = 10$ experiments, two-way ANOVA with Bonferroni's post hoc test; $^{**}P < 0.01$ and $^{***}P < 0.001$). (**B**) Uptake of FITC-albumin in *Trpv4*$^{+/+}$ and *Trpv4*$^{-/-}$ mPTCs in the absence or in the presence of 100 nM GSK1016790A. Uptake of FITC-albumin was assessed at 37°C for 15 min. The intensity of FITC-fluorescence of cell lysates was quantified by fluorophotometry. (**C**) FITC-albumin uptake in mPTCs in Ca^{2+}-containing or in Ca^{2+}-free medium in the absence or in the presence of GSK1016790A ($n = 10$ experiments, two-way ANOVA with Bonferroni post hoc test; $^{**}P < 0.01$ and $^{***}P < 0.001$). (**D**) Quantification of albumin uptake in mPTCs from *Trpv4*$^{+/+}$ and *Trpv4*$^{-/-}$ mice incubated for 1 hour at 37°C with FITC-labeled albumin under basal conditions, stretched conditions, and stretched in the presence of the TRPV4 antagonist HC067047 1 μM (HC; $n = 15$ fields for each condition from three mice; two-way ANOVA with Bonferroni post hoc test; $^{*}P < 0.05$ and $^{**}P < 0.01$). A.U., arbitrary units. (**E**) Representative fluorescence images of mPTCs from *Trpv4*$^{+/+}$ and *Trpv4*$^{-/-}$ mice incubated for 1 hour at 37°C with FITC-labeled albumin under basal and stretched conditions ($n = 3$ mPTC culture for each group). (**F**) *Trpv4*$^{+/+}$ mPTCs were incubated with FITC-albumin (5 min, 0.5 mg/ml, 37°C, green) in the presence of GSK1016790A and immunostained with anti–Rab-7 antibody (red; $n = 3$ mPTC cultures). (**G**) *Trpv4*$^{+/+}$ mPTCs were incubated with FITC-albumin (35 min, 0.5 mg/ml, 37°C, green) in the presence of GSK1016790A and immunostained with anti–lysosomal-associated membrane protein 1 (LAMP1) antibody (red). Hoechst (blue) counterstaining of the nucleus ($n = 3$ mPTC cultures). Scale bars, 10 μm.

AT2 infusion has a strong effect on glomerular permeability and is associated with many side effects (such as hypertension and vascular disease). Moreover, TRPV4 is expressed in different segments of the nephron (*40*), making it difficult to discriminate its specific contribution in the PT. To deal with both issues, we used a milder and more pathophysiologically relevant protocol to impair glomerular permeability, and we created mice in which *Trpv4* was deleted specifically in the PT. We crossed *Trpv4*$^{lox/-}$ mice to mice expressing the Cre-recombinase under the promoter of the phosphoenolpyruvate carboxykinase (PEPCK) (*43*) and compared *Trpv4*$^{lox/-}$ *PEPCK-Cre*$^{+/-}$ (hereinafter referred to as cKO) to their *Trpv4*$^{lox/-}$ *PEPCK-Cre*$^{-/-}$ littermates (hereinafter referred to as control; Fig. 7A). Immunostaining in kidney sections from control mice revealed megalin in the PT and TRPV4 in the PTs and in the distal convoluted tubules, confirming a distribution pattern of TRPV4 similar to that which we observed previously in *Trpv4*$^{+/+}$ mice (*40*) (Fig. 7B). We confirmed that the *Tomato* reporter gene was specifically expressed in the PT of cKO mice and that the expression of TRPV4 was specifically reduced in the PT but not in other segments of the nephron of cKO mice (Fig. 7, C and D). We next intravenously injected these mice with serum containing antibodies directed against the glomerular and/or pulmonary basement membrane (anti-GBM serum). Anti-GBM disease is a rare cause of glomerulonephritis, similar to that seen in Goodpasture's syndrome (*44*), characterized by the presence of autoantibodies directed at specific antigenic targets within the glomerular and/or pulmonary basement membrane. These antibodies bind to the α3 chain of type IV collagen found in these specialized basement membranes (*45*). Anti-GBM serum–treated cKO mice showed a significant increase in proteinuria compared with control mice (Fig. 7E) and an increase in diuresis that was not statistically significant (Fig. 7F). We did not observe changes in glycosuria and phosphaturia after anti-GBM treatment (Fig. 7, G and H).

DISCUSSION

Our data showed that TRPV4 was expressed in cultured PT cells and could be activated by the specific agonist GSK1016790A and by hypotonic

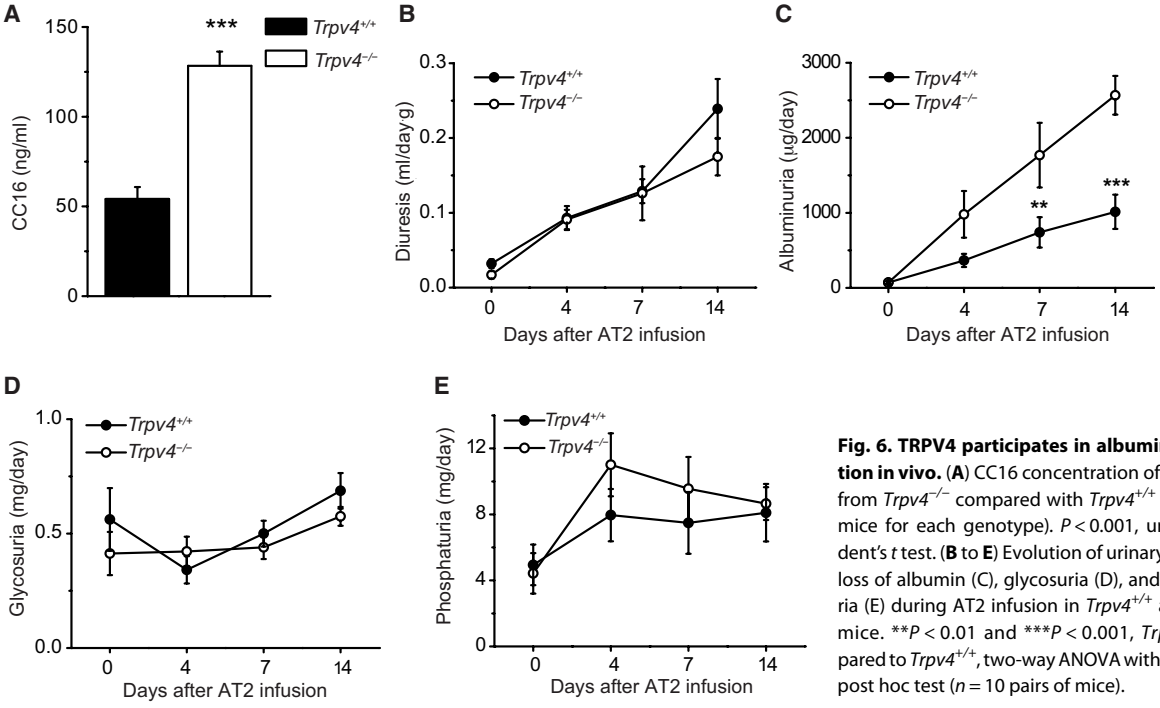

Fig. 6. TRPV4 participates in albumin reabsorption in vivo. (**A**) CC16 concentration of basal urines from $Trpv4^{-/-}$ compared with $Trpv4^{+/+}$ mice ($n = 10$ mice for each genotype). $P < 0.001$, unpaired Student's t test. (**B** to **E**) Evolution of urinary diuresis (B), loss of albumin (C), glycosuria (D), and phosphaturia (E) during AT2 infusion in $Trpv4^{+/+}$ and $Trpv4^{-/-}$ mice. $^{**}P < 0.01$ and $^{***}P < 0.001$, $Trpv4^{-/-}$ compared to $Trpv4^{+/+}$, two-way ANOVA with Bonferroni's post hoc test ($n = 10$ pairs of mice).

solution. In kidney slices, TRPV4 was detected almost exclusively at the basolateral side of PT cells. As expected, the entry of Ca^{2+} in response to shear stress was therefore not affected in mPTCs from $Trpv4^{-/-}$ mice. However, Ca^{2+} entry was observed in mPTCs in response to stretch caused by deformation of silicon stretchable chambers, and this Ca^{2+} influx was reduced in $Trpv4^{-/-}$ PT cells. We did not observe differences between $Trpv4^{+/+}$ and $Trpv4^{-/-}$ mPTCs in response to membrane stretch. In particular, SAC activity in mPTCs was almost completely inhibited by GsMTx-4, suggesting that Piezo channels, which are sensitive to this toxin, play a critical role in these stretch-activated currents. Piezo1 can be directly gated by lipid bilayer tension (*46*), which might not be sufficient for TRPV4. Different molecular mechanisms have been proposed for the mechanical gating of TRPV4. TRPV4 has been proposed to be directly activated by membrane stretch, but in contrast to what is observed in *Xenopus laevis* oocytes, TRPV4 overexpressed in mammalian cells does not respond to pressure-clamp stimulation (*31*, *47*). The mechanical activation of TRPV4 could be downstream of a phospholipase A_2 (PLA2)–dependent pathway, as observed after osmotic stimulus, and shear stress causes an endothelial cell–dependent vasodilation through PLA2 and TRPV4 activation (*48*). TRPV4 could be directly activated through deformation of intracellular, transmembrane, or extracellular linking proteins. In this context, ultrarapid activation of TRPV4 (within milliseconds) has been observed by magnetically twisting β-integrin in adherens junctions (*49*), and TRPV4 has been detected in the adherens junctions in urothelium (*22*) and in intercellular junctions between keratinocytes (*50*).

Our results support the notion that membrane stretch and substrate stretch stimulate different mechanical pathways in mPTCs. They also agree with a study showing that the most effective stimulus to open TRPV4 is membrane deformation at a cell-substrate contact point, which has a latency of <2 ms and is independent of PLA2 activity (*23*), suggesting direct mechanical gating.

Consistent with this study (*23*), we hypothesize that the strain of silicon chambers is an effective way to gate TRPV4 in epithelial PT cells because the stimulus is applied at cell-substrate contact points. However, the identity and the functions of the putative tethers are still to be determined.

The secondary structure of TRPV4 (*51*) and its crystal structure (*52*) show that a large subset of disease-causing mutations are segregated at the outer perimeter of the tetrameric channel, suggesting that the interactions between TRPV4 and protein partners or signaling molecules are crucial for the physiological function of TRPV4. Alteration in these interactions could be a factor affecting many disease phenotypes.

The modulation of PT functions by the amount of ultrafiltrate delivered to the PT suggests the presence of mechanotransduction structures. Two types of force are theoretically developed by the entry of the ultrafiltrate in the PT lumen: a shear stress on the apical membrane and a radial stretch on the basolateral or apical sides of PT cells (*4*, *11*, *53*). An increase in glomerular filtration leads to increased fluid shear stress on PT cells that enables the reabsorption of Na^+ and HCO_3^- ions (*54*) and the expression of the water channel AQP1 (*55*). Moreover, shear stress has been suggested to enhance endocytosis in PT cells in a Ca^{2+}- and cilium-dependent manner (*10*, *56*). However, Delling *et al.* (*57*) showed that primary cilia from the kidney are not Ca^{2+}-sensitive mechanosensors. For this reason, further advances in our understanding the relationship between Ca^{2+} signals and mechanical modulation of endocytosis is still needed. In isolated perfused PTs and in unilateral obstruction disease models, increased flow in the PT induces a change in the outer diameter of the tubule and the lumen. However, it is so far unclear whether such changes appear under physiological flow variations (*4*). Mechanical stretch of PT cells triggers a β-integrin–dependent reinforcement of focal adhesions and an increase in $[Ca^{2+}]_i$ [reviewed in (*58*)]. The presence of SACs on PTCs has been

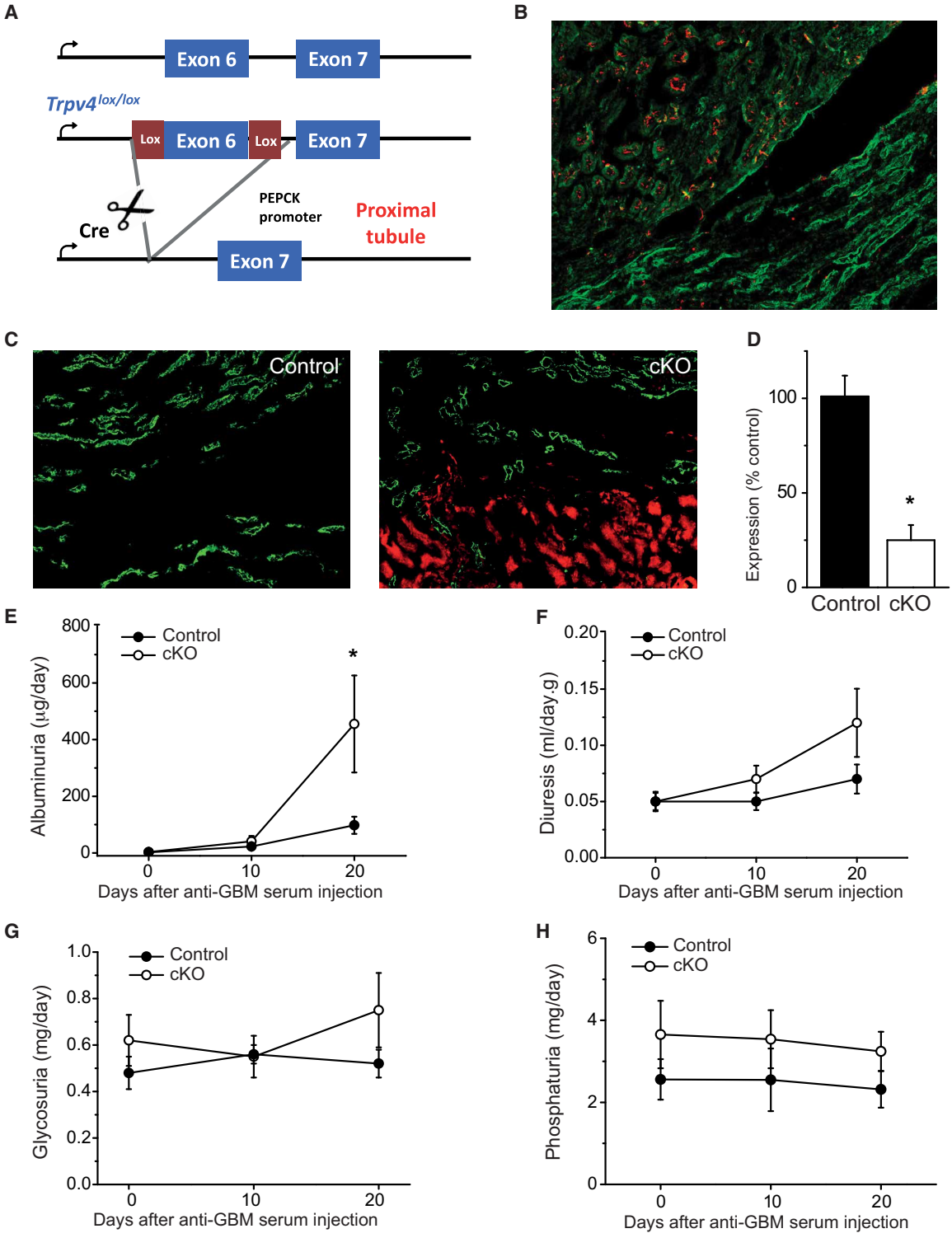

Fig. 7. Albumin reabsorption in cKO mice. (**A**) Mice with the sixth exon of *Trpv4* gene flanked with loxP sites (middle line) were bred with PEPCK-Cre recombinase mice to obtain PT-specific conditional *Trpv4* knockout mice (bottom line). (**B**) Coimmunolabeling of TRPV4 (in green) and megalin (red) on renal cortex sections from *Trpv4*$^{lox/-}$ *PEPCK-Cre*$^{-/-}$ (control) mice ($n = 8$ kidney sections). (**C**) Coimmunolabeling of AQP2 (in green) and tomato (red) on renal cortex sections from *Trpv4*$^{lox/-}$ *PEPCK-Cre*$^{-/-}$ (control) and *Trpv4*$^{lox/-}$ *PEPCK-Cre*$^{+/-}$ (cKO) mice ($n = 5$ kidney sections for each genotype). (**D**) *Trpv4* expression measured by qRT-PCR analysis in PT fragments obtained after digestion and filtration of renal cortices isolated from cKO and control mice ($n = 3$ samples from three different mice for each genotype). *$P < 0.05$, Student's *t* test. (**E** to **H**) Evolution of urinary loss of albumin (E), diuresis (F), glycosuria (G), and phosphaturia (H) before and after injection of 200 µl of anti-GBM serum in control and cKO mice ($n = 9$ mice for each genotype). *$P < 0.05$, cKO compared with control, two-way ANOVA with Bonferroni's post hoc test.

suggested by Alexander and colleagues (*59*), who showed that cyclic stretch of isolated PTCs activates PLA2 and ERKs (extracellular signal–regulated kinases) through a mechanism that depends on external Ca^{2+} and is blocked by Gd^{3+}. Here, we observed that TRPV4 was mainly expressed at the basolateral side of the PT and that uptake of FITC-labeled albumin was increased when TRPV4 was activated pharmacologically or mechanically in a manner that depends on the entry of Ca^{2+} in PT cells. The TRPV4 agonist GSK1016790A increased the V_{max} value but did not affect K_m values for transport.

We showed that *Trpv4*$^{-/-}$ mice presented with a higher urinary concentration of CC16, a sensitive marker of PT dysfunction (*41*). Moreover, mice with altered glomerular filter function due to continuous delivery of AT2 or to acute injection of anti-GBM serum developed albuminuria that was more pronounced in *Trpv4*$^{-/-}$ mice than in WT mice. These results suggest the importance of the process in diseases accompanied by altered permeability characteristics of the glomerular filter, some being very rare such as the Goodpasture's syndrome (see above), and some being very common such as the diabetic nephropathy (*60*). PT dysfunction is itself involved in various forms of the Fanconi syndrome, which is often associated with rare inherited diseases such as Dent's disease (*61*, *62*) or disease states accompanied by intraluminal pressure increases, such as obstructive uropathy (*56*, *63*–*65*) or polycystic kidney disease (*66*). We therefore hope that our finding that radial stretch of the PT is sensed by basolateral TRPV4, which modifies albumin reabsorption, will help to treat patients with proteinuria. Future studies will be needed to investigate whether a deficit in TRPV4-mediated endocytosis contributes to kidney diseases with tubular proteinuria.

MATERIALS AND METHODS

Generation of *Trpv4* conditional knockout mice

Trpv4$^{-/-}$ mice were generated using AK7 mouse embryonic stem cells. The *Trpv4* gene was targeted by homologous recombination with a construct from the International Knockout (KO) Mice Consortium that bears *loxP* sites flanking the sixth exon (ID: 79331) (*49*). After selection of several correctly targeted clones, we injected them into C57BL/6J mice host blastocysts. The embryos were transferred into pseudopregnant CD1 mice. Chimeric male offspring were selected on the basis of the coat color. They were mated with C57BL/6J females to assess the transmission of the targeted allele. Mice harboring the targeted allele were mated with *ROSA-Flp* females to excise the selection cassette. The resulting mice had the sixth exon of the *Trpv4* gene flanked with *loxP* sites (*Trpv4lox*). *Trpv4*$^{lox/lox}$ mice were crossed with a mouse line expressing the Cre recombinase under the *Phosphoglycerate kinase 1* (*PGK-1*) promoter to obtain a constitutive *Trpv4* KO mouse line (*Trpv4*$^{-/-}$). Loss of expression of TRPV4 in *Trpv4*$^{-/-}$ mice was assessed by quantitative reverse transcription polymerase chain reaction (qRT-PCR), by Western blotting on kidney or PT extracts, and by immunohistochemistry (Fig. 1, A to C).

To obtain the conditional *Trpv4* KO mouse model, mice with the *Trpv4lox* allele were bred with *Trpv4*$^{-/-}$ mice heterozygous for the *ROSA26-lox-stop-lox-tdTomato* reporter gene to obtain the *Trpv4*$^{lox/-}$ *Tom*^{lox} genotype. To achieve deletion specifically in PTs, *Trpv4*$^{lox/-}$ mice were crossed with mice expressing the Cre fusion protein under the control of the regulatory elements of the *PEPCK* gene (*PEPCK-Cre* transgene) (*43*). Heterozygous transgenic mice *Trpv4*$^{lox/-}$ *Tom*$^{lox/-}$ *PEPCK-Cre*$^{+/-}$ and their *Trpv4*$^{lox/-}$ *Tom*$^{lox/-}$ *PEPCK-Cre*$^{-/-}$ littermates were identified by PCR genotyping.

Ethical approval

All animals were housed and handled according to the Belgian Council on Animal Care guidelines based on protocols approved by the Animal Ethics Committee of the Université catholique de Louvain (2017/UCL/MD013 and 2020/UCL/MD/015). Animals were given access to food and water ad libitum unless otherwise stated. At appropriate experimental time points, all animals were humanely euthanized by an overdose of anesthetic followed by decapitation.

Immunostaining

Trpv4$^{+/+}$ and *Trpv4*$^{-/-}$ mice were deeply anesthetized by intraperitoneal injection (10 ml/kg) of a solution containing ketamine (10 mg/ml) and xylazine (1 mg/ml). After intracardiac perfusion with a 4°C buffered 4% paraformaldehyde phosphate-buffered saline (PBS) solution, kidneys were removed and postfixed in the same solution for 2 hours, washed in PBS, and cryoprotected overnight in 30% sucrose PBS. After embedding in optimal cutting temperature compound (Tissue-Tek, VWR), 10-μm-thick cryosections were cut and stored at −80°C. Sections were blocked with a 3% bovine serum albumin (BSA) containing PBS solution and then incubated overnight with the following antibodies: 1/200 anti-TRPV4 (Alomone), 1/200 anti-Aquaporin 2 (Sigma-Aldrich), 1/200 anti-megalin (generated in house), 1/100 anti-Na^+/K^+-ATPase (Sigma-Aldrich), 1/200 anti-Lamp1 (Abcam), 1/200 anti-Rab7 (Abcam), and subsequently with Alexa Fluor 488 or 568 (Thermo Fisher Scientific). DAPI (4′,6-diamidino-2-phenylindole) (Thermo Fisher Scientific) was used for nuclear staining. Images were acquired with an Olympus FV1000 confocal microscope.

Real-time PCR

Total RNAs from whole kidney, PTs, and PT cells were extracted using TRIzol reagent (Invitrogen) according to the manufacturer's protocol and reverse transcribed using qScript Reverse Transcriptase (Quanta Biosciences, Gaithersburg, ME). Complementary DNA (cDNA)–specific PCR primers were designed using Primer-BLAST (table S2) and purchased from Eurogentec (Seraing, Belgium). Gapdh was used as reference gene. qRT-PCR was performed using SYBRGreen Mix (Bio-Rad, Hercules, CA, USA). The reaction was initiated at 95°C for 3 min, followed by 40 cycles of denaturation at 95°C for 10 s, annealing at 60°C for 1 min, and extension at 72°C for 10 s. Data were recorded on an MyiQ qPCR detection system (Bio-Rad), and cycle threshold (*C*t) values for each reaction were determined using analytical software from the same manufacturer. Each cDNA was amplified in duplicate, and *C*t values were averaged for each duplicate. The average *C*t value for *Gapdh*, which was selected as the reference gene, was subtracted from the average *C*t value for the gene of interest. The Δ*C*t value was then subtracted from the Δ*C*t value obtained in control cells, giving a ΔΔ*C*t value. Because amplification efficiencies of primer pairs were comparable, the *Gapdh*-normalized expression of mRNAs was given by the relation $2^{-\Delta\Delta Ct}$.

Western blotting

Cells were collected in radioimmunoprecipitation assay (RIPA) buffer [25 mM tris HCl (pH 7.6), 150 mM NaCl, 1% NP-40, 1% sodium deoxycholate, and 0.1% SDS]. Thirty micrograms of protein for each sample was loaded on a 10% SDS–polyacrylamide gel,

transferred to a polyvinylidene difluoride (PVDF) membrane, and probed with the following antibodies: an anti-TRPV4 antibody described earlier (*67*), an anti-aquaporin 1 antibody (Sigma-Aldrich) as a positive marker for the PT, an anti–aquaporin 2 antibody (Sigma-Aldrich) as a negative marker of PT (*40*), and an anti–glyceraldehyde-3-phosphate dehydrogenase (GAPDH) antibody as loading control (Cell Signaling Technology).

Primary culture of mPTCs

Male *Trpv4*$^{+/+}$ and *Trpv4*$^{-/-}$ mice were decapitated, and kidneys were removed and decapsulated. The dissection was done as described previously (*37*, *40*). Renal cortices were dissected in Hanks' balanced salt solution (HBSS) and sliced into pieces of ~1 mm wide. The fragments were transferred to a collagenase solution [HBSS with 0.1% type 2 collagenase and soybean trypsin inhibitor (96 μg/ml)] at 37°C and digested for 30 min. After digestion, the supernatant was filtered through two nylon sieves (pore sizes of 250 and 80 μm) to obtain a large number of long PT fragments without substantial contamination of other nephron segments or glomeruli. The longer PT fragments that remained in the 80-μm sieve were resuspended with warm HBSS (37°C) containing BSA 1% (w/v). The PTs present in the BSA solution were centrifuged for 5 min at 170*g*, washed, and then resuspended into the appropriate amount of culture medium: 1:1 Dulbecco's modified Eagle's medium (DMEM)/F12 (Gibco) without phenol red and supplemented with heat-inactivated 1% fetal calf serum (FCS), 15 mM Hepes, 2 mM L-glutamine, 50 nM hydrocortisone, insulin (5 μg/ml), transferrin (5 μg/ml), 50 nM selenium, 0.55 mM sodium pyruvate, 100× nonessential amino acids (10 ml/liter), penicillin (100 IU/ml), and streptomycin (100 μg/ml; Thermo Fisher Scientific). The solution was buffered to pH 7.4 and adjusted to an osmolality of 325 mOsm. The PT fragments were seeded onto collagen-coated coverslips and left unstirred for 48 hours in a standard humidified incubator. The medium was then replaced every 2 days. After 7 days, cell cultures were organized as a confluent monolayer. No differences in cell shape and size or in proliferation were observed between *Trpv4*$^{-/-}$ and *Trpv4*$^{+/+}$ mPTCs.

Ca^{2+} imaging

Loading of the mPTCs with Fura2-AM (Thermo Fisher Scientific) was achieved at room temperature in Krebs medium with 5 μM Fura2-AM and 0.01% pluronic acid for 1 hour. $[Ca^{2+}]_i$ was measured in 15 to 20 individual cells using alternative excitation of Fura2-AM (0.5 Hz) at 340 and 380 nm using a Lambda DG-4 Ultra High Speed Wavelength Switcher (Sutter Instrument, Novato, CA, USA). Images were acquired with a Zeiss Axiocam camera coupled to a 510-nm emission filter and analyzed with Axiovision software. Ca^{2+} imaging experiments were performed in Krebs-Hepes solution [135 mM NaCl, 5.9 mM KCl, 1.2 mM $MgCl_2$, 1.8 mM $CaCl_2$, 11.6 mM Hepes, 11.5 mM glucose (pH 7.35)]. For hypotonic shock experiments, cells were bathed in a modified Krebs-Hepes solution where NaCl was partially omitted in the hypotonic solution (170 mOsm) or replaced by mannitol in the isotonic solution (310 mOsm), to avoid changes in ionic gradients. For shear stress experiments, flow was applied on cells with an 18-gauge needle connected to a peristaltic pump perfusion system and placed above the field. For measurement of $[Ca^{2+}]_i$ during cell stretching, cells were passaged on collagen I–coated flexible silicon chambers (ST-CH-04, B-Bridge), placed on the microscope-mountable stretching instrument (ST-150, B-Bridge), and strained for 1 s by 20% uniaxial stretching (*27*).

Electrophysiological recordings

Patch-clamp recordings of mPTCs were carried out at room temperature using an EPC-9 amplifier (HEKA Elektronik, Lambrecht, Germany) controlled by PatchMaster software (HEKA Elektronik, Lambrecht, Germany). Patch-clamp electrodes were pulled and fire polished to 3.0 ± 0.5 Megohm resistance for whole-cell experiments and 2.0 ± 0.5 Megohms for pressure-clamp experiments using a DMZ-Universal Puller (Zeitz Instruments, Munich, Germany). An AgCl wire was used as a reference electrode. Series resistance was electronically compensated. Whole-cell currents of mPTCs were acquired using repetitive 400-ms voltage ramps (at 2-s intervals) from −120 to +120 mV, applied from a holding potential of 0 mV. Currents were sampled at 20 kHz and digitally filtered at 2.9 kHz. For statistical analysis, the currents were normalized to cell capacitance. Solutions were applied to the cells with a home-made gravity-fed perfusion system connected by a five-way manifold to an RC25 perfusion chamber (Warner Instruments, Hamden, CT, USA). For whole-cell recordings, the standard extracellular solution had the following composition: 150 mM NaCl, 5 mM CsCl, 1 mM $MgCl_2$, 1.8 mM $CaCl_2$, 10 mM glucose, and 10 mM Hepes, buffered at pH 7.4 with NaOH. The osmolarity of this solution was 320 ± 5 mOsm/kg H_2O. For hypotonic cell swelling, we superfused mPTCs with a solution containing 105 mM NaCl, 5 mM CsCl, 1 mM $MgCl_2$, 1.8 mM $CaCl_2$, 10 mM glucose, 80 mannitol, and 10 mM Hepes, buffered to pH 7.4 with NaOH (320 ± 5 mOsm). Hypotonic cell swelling was induced by removing mannitol to lower the extracellular osmolarity to 240 ± 5 mOsm. For hypotonic cell swelling in a low-chloride containing extracellular solution, 105 mM NaCl was replaced by 105 mM Na-aspartate. The pipette solution was composed of 40 mM CsCl, 100 mM Cs-aspartate, 1 mM $MgCl_2$, 10 mM Hepes, 4 mM Na_2ATP, 10 mM EGTA, and 0.5 mM $CaCl_2$, adjusted to pH 7.2 with CsOH (290 ± 5 mOsm). For pressure-clamp recordings on mPTCs, we used the following pipette solution, as previously described (*13*): 150 mM NaCl, 5 mM KCl, 2 mM $CaCl_2$, and 10 mM Hepes (pH 7.4 with NaOH). The pipette solution also contained 10 mM Tetraethylammonium (TEA), 5 mM 4-aminopyridine, and 10 μM glibenclamide to inhibit K^+ channels. The bath medium contained the following: 155 mM KCl, 5 mM EGTA, 3 mM $MgCl_2$, and 10 mM Hepes (pH 7.2 with KOH), to zero the membrane potential. Membrane patches in cell-attached configuration were stimulated, at the holding potential of −80 mV, with 300-ms negative pressure pulses from 0 to −80 mmHg (10 mmHg steps, at 4-s intervals), using a fast pressure-clamp device (ALA High Speed Pressure Clamp-1 System, ALAScientific). Data and statistical analysis were performed using Origin 8.0 (OriginLab Corporation, Northampton, MA). GSK1016790A, HC067047, GsMTx-4, OBAA, and DIDS were obtained from Tocris Bioscience.

Albumin and dextran uptake assay

For endocytosis experiments, mPTCs were cultured on collagen-coated polytetrafluoroethylene membranes (pore size of 0.4 μm). We previously showed that these cells are polarized with numerous microvilli, basolateral invaginations, and apical tight junctions (*37*). They express only PT-specific proteins and, in particular, the components of the receptor-mediated endocytic pathway, the PT brush-border enzymes (alkaline phosphatase and glutamyl-transferase), and the phloridzin-sensitive sodium-dependent glucose transport (SGLT2) on the apical membrane. However, these cells kept a flat morphology, and asymmetry of the apical compared with basolateral

distribution of TRPV4 could not be demonstrated using immunostaining and confocal microscopy.

mPTCs were serum starved overnight and incubated with FITC-labeled albumin (0.5 mg/ml; Sigma-Aldrich) or FITC-labeled dextran (1 mg/ml; Sigma-Aldrich) in DMEM/F12 medium for 30 min at 37°C. The cells were washed with cold PBS five times and lysed in PBS with 0.1% Triton-X. The supernatant was used for fluorescence and protein assays. The intensity of FITC-fluorescence was measured by fluorophotometry. For the study of albumin endocytosis during cell stretching, cells were seeded on collagen I–coated flexible silicon chambers (ST-CH-10, B-Bridge) and placed in the stretching instrument (ST-140, B-Bridge). A uniaxial stretching of 20% was applied at a frequency of 0.3 Hz. At the end of the experiments, the cells were washed five times with ice-cold PBS, and fluorescence signals were immediately assessed using a fluorescence microscope.

AT2 infusion studies

Infusion of AT2 (Tocris) at a dose of 1 ng/g per minute dissolved in sterile saline for 14 days was performed with osmotic minipumps (Alzet model 2004; Alza Corp., Mountain View, CA) (*42*). The pumps were implanted subcutaneously in the dorsal region under ketamine-xylazine anesthesia (100 to 10 μg/g). After a recovery period of 4 days, urine was collected over a 24-hour period at 4, 7, and 14 days postimplantation in metabolic cages.

Anti-GMB serum treatment

To induce progressive glomerulonephritis, 200 μl of anti-GBM serum (sheep anti-rat glomeruli serum, Probetex, Inc.) was administered to 6- to 8-week-old mice by tail vein injection. Urine samples were collected on days 1, 10, and 20 after antiserum injection. On day 20, the mice were euthanized to collect plasma and kidney tissue.

Urine analysis

Urine samples were centrifuged to remove debris, weighed, and frozen at −80°C. Urine samples were quantified for albumin (ab108792 ELISA kit, Abcam), glucose (Fuji Dri-Chem NX500 analyzer), phosphate (Phosphate Assay Kit, Abcam), creatinine (QuantiChrom Creatinine Assay Kit, BioAssay Systems), and CC16 (Cloud-Clone Corp.).

Statistical analysis

All values are expressed as means ± SEM. Paired *t* test was used to assess statistical differences between two groups, and analysis of variance (ANOVA) with Bonferroni's test was used for multiple group comparisons. Statistical significance was indicated if $P < 0.05$.

SUPPLEMENTARY MATERIALS

stke.sciencemag.org/cgi/content/full/13/653/eabc6967/DC1

Fig. S1. Complete versions of Western blots presented in Fig. 1.

Fig. S2. Capacitance of mPTCs from *Trpv4*$^{+/+}$ and *Trpv4*$^{-/-}$ mice.

Fig. S3. Effect of OBAA on stretch-induced Ca^{2+} entry in mPTCs.

Fig. S4. Dextran uptake induced by TRPV4 activation in mPTCs.

Fig. S5. Creatinine clearance of mice treated with AT2.

Fig. S6. AT2-induced proteinuria is not caused by down-regulation of genes involved in endocytosis.

Table S1. K_m and V_{max} values extrapolated from Michaelis-Menten kinetics analysis.

Table S2. List of DNA primers used in quantitative RT-PCR.

View/request a protocol for this paper from *Bio-protocol*.

REFERENCES AND NOTES

1. E. I. Christensen, P. J. Verroust, R. Nielsen, Receptor-mediated endocytosis in renal proximal tubule. *Pflugers Arch.* **458**, 1039–1048 (2009).
2. O. Devuyst, A. Luciani, Chloride transporters and receptor-mediated endocytosis in the renal proximal tubule. *J. Physiol.* **593**, 4151–4164 (2015).
3. M. L. Eshbach, O. A. Weisz, Receptor-mediated endocytosis in the proximal tubule. *Annu. Rev. Physiol.* **79**, 425–448 (2017).
4. V. Raghavan, O. A. Weisz, Discerning the role of mechanosensors in regulating proximal tubule function. *Am. J. Physiol. Renal Physiol.* **310**, F1–F5 (2016).
5. J. Kim, C. L. Bronson, W. L. Hayton, M. D. Radmacher, D. C. Roopenian, J. M. Robinson, C. L. Anderson, Albumin turnover: FcRn-mediated recycling saves as much albumin from degradation as the liver produces. *Am. J. Physiol. Gastrointest. Liver Physiol.* **290**, G352–G360 (2006).
6. B.-C. Liu, T.-T. Tang, L.-L. Lv, H.-Y. Lan, Renal tubule injury: A driving force toward chronic kidney disease. *Kidney Int.* **93**, 568–579 (2018).
7. J. van der Wijst, H. Belge, R. J. M. Bindels, O. Devuyst, Learning physiology from inherited kidney disorders. *Physiol. Rev.* **99**, 1575–1653 (2019).
8. R. Nielsen, E. I. Christensen, Proteinuria and events beyond the slit. *Pediatr. Nephrol.* **25**, 813–822 (2010).
9. Y. Duan, A. M. Weinstein, S. Weinbaum, T. Wang, Shear stress-induced changes of membrane transporter localization and expression in mouse proximal tubule cells. *Proc. Natl. Acad. Sci. U.S.A.* **107**, 21860–21865 (2010).
10. V. Raghavan, O. A. Weisz, Flow stimulated endocytosis in the proximal tubule. *Curr. Opin. Nephrol. Hypertens.* **24**, 359–365 (2015).
11. M. C. Drumond, W. M. Deen, Analysis of pulsatile pressures and flows in glomerular filtration. *Am. J. Physiol.* **261**, F409–F419 (1991).
12. B. Martinac, K. Poole, Mechanically activated ion channels. *Int. J. Biochem. Cell Biol.* **97**, 104–107 (2018).
13. R. Peyronnet, J. R. Martins, F. Duprat, S. Demolombe, M. Arhatte, M. Jodar, M. Tauc, C. Duranton, M. Paulais, J. Teulon, E. Honoré, A. Patel, Piezo1-dependent stretch-activated channels are inhibited by Polycystin-2 in renal tubular epithelial cells. *EMBO Rep.* **14**, 1143–1148 (2013).
14. J. P. M. White, M. Cibelli, L. Urban, B. Nilius, J. G. McGeown, I. Nagy, TRPV4: Molecular conductor of a diverse orchestra. *Physiol. Rev.* **96**, 911–973 (2016).
15. S. Ciura, M. Prager-Khoutorsky, Z. S. Thirouin, J. C. Wyrosdic, J. E. Olson, W. Liedtke, C. W. Bourque, Trpv4 mediates hypotonic inhibition of central osmosensory neurons via taurine gliotransmission. *Cell Rep.* **23**, 2245–2253 (2018).
16. H. Matsumoto, S. Sugio, F. Seghers, D. Krizaj, H. Akiyama, Y. Ishizaki, P. Gailly, K. Shibasaki, Retinal detachment-induced muller glial cell swelling activates TRPV4 ion channels and triggers photoreceptor death at body temperature. *J. Neurosci.* **38**, 8745–8758 (2018).
17. K. Shibasaki, K. Ikenaka, F. Tamalu, M. Tominaga, Y. Ishizaki, A novel subtype of astrocytes expressing TRPV4 (transient receptor potential vanilloid 4) regulates neuronal excitability via release of gliotransmitters. *J. Biol. Chem.* **289**, 14470–14480 (2014).
18. K. Shibasaki, S. Sugio, K. Takao, A. Yamanaka, T. Miyakawa, M. Tominaga, Y. Ishizaki, TRPV4 activation at the physiological temperature is a critical determinant of neuronal excitability and behavior. *Pflugers Arch.* **467**, 2495–2507 (2015).
19. U. Wissenbach, M. Bödding, M. Freichel, V. Flockerzi, Trp12, a novel Trp related protein from kidney. *FEBS Lett.* **485**, 127–134 (2000).
20. M. Suzuki, A. Mizuno, K. Kodaira, M. Imai, Impaired pressure sensation in mice lacking TRPV4. *J. Biol. Chem.* **278**, 22664–22668 (2003).
21. R. Masuyama, J. Vriens, T. Voets, Y. Karashima, G. Owsianik, R. Vennekens, L. Lieben, S. Torrekens, K. Moermans, A. V. Bosch, R. Bouillon, B. Nilius, G. Carmeliet, TRPV4-mediated calcium influx regulates terminal differentiation of osteoclasts. *Cell Metab.* **8**, 257–265 (2008).
22. T. Suzuki, T. Notomi, D. Miyajima, F. Mizoguchi, T. Hayata, T. Nakamoto, R. Hanyu, P. Kamolratanakul, A. Mizuno, M. Suzuki, Y. Ezura, Y. Izumi, M. Noda, Osteoblastic differentiation enhances expression of TRPV4 that is required for calcium oscillation induced by mechanical force. *Bone* **54**, 172–178 (2013).
23. M. R. Servin-Vences, M. Moroni, G. R. Lewin, K. Poole, Direct measurement of TRPV4 and PIEZO1 activity reveals multiple mechanotransduction pathways in chondrocytes. *eLife* **6**, e21074 (2017).
24. D. A. W. Janssen, J. G. Hoenderop, K. C. F. J. Jansen, A. W. Kemp, J. P. F. A. Heesakkers, J. A. Schalken, The mechanoreceptor TRPV4 is localized in adherence junctions of the human bladder urothelium: A morphological study. *J. Urol.* **186**, 1121–1127 (2011).
25. M. Kottgen, B. Buchholz, M. A. Garcia-Gonzalez, F. Kotsis, X. Fu, M. Doerken, C. Boehlke, D. Steffl, R. Tauber, T. Wegierski, R. Nitschke, M. Suzuki, A. Kramer-Zucker, G. G. Germino, T. Watnick, J. Prenen, B. Nilius, E. W. Kuehn, G. Walz, TRPP2 and TRPV4 form a polymodal sensory channel complex. *J. Cell Biol.* **182**, 437–447 (2008).
26. L. Wu, X. Gao, R. C. Brown, S. Heller, R. G. O'Neil, Dual role of the TRPV4 channel as a sensor of flow and osmolality in renal epithelial cells. *Am. J. Physiol. Renal Physiol.* **293**, F1699–F1713 (2007).
27. F. Seghers, X. Yerna, N. Zanou, O. Devuyst, R. Vennekens, B. Nilius, P. Gailly, TRPV4 participates in pressure-induced inhibition of renin secretion by juxtaglomerular cells. *J. Physiol.* **594**, 7327 (2016).

28. B. P. Festa, Z. Chen, M. Berquez, H. Debaix, N. Tokonami, J. A. Prange, G. van de Hoek, C. Alessio, A. Raimondi, N. Nevo, R. H. Giles, O. Devuyst, A. Luciani, Impaired autophagy bridges lysosomal storage disease and epithelial dysfunction in the kidney. *Nat. Commun.* **9**, 161 (2018).
29. J. Berrout, M. Jin, M. Mamenko, O. Zaika, O. Pochynyuk, R. G. O'Neil, Function of transient receptor potential cation channel subfamily V member 4 (TRPV4) as a mechanical transducer in flow-sensitive segments of renal collecting duct system. *J. Biol. Chem.* **287**, 8782–8791 (2012).
30. W. Liedtke, Y. Choe, M. A. Martí-Renom, A. M. Bell, C. S. Denis, A. Sali, A. J. Hudspeth, J. M. Friedman, S. Heller, Vanilloid receptor-related osmotically activated channel (VR-OAC), a candidate vertebrate osmoreceptor. *Cell* **103**, 525–535 (2000).
31. R. Strotmann, C. Harteneck, K. Nunnenmacher, G. Schultz, T. D. Plant, OTRPC4, a nonselective cation channel that confers sensitivity to extracellular osmolarity. *Nat. Cell Biol.* **2**, 695–702 (2000).
32. J. Vriens, H. Watanabe, A. Janssens, G. Droogmans, T. Voets, B. Nilius, Cell swelling, heat, and chemical agonists use distinct pathways for the activation of the cation channel TRPV4. *Proc. Natl. Acad. Sci. U.S.A.* **101**, 396–401 (2004).
33. B. Nilius, J. Eggermont, T. Voets, G. Buyse, V. Manolopoulos, G. Droogmans, Properties of volume-regulated anion channels in mammalian cells. *Prog. Biophys. Mol. Biol.* **68**, 69–119 (1997).
34. N. Ullrich, A. Caplanusi, B. Brône, D. Hermans, E. Larivière, B. Nilius, W. Van Driessche, J. Eggermont, Stimulation by caveolin-1 of the hypotonicity-induced release of taurine and ATP at basolateral, but not apical, membrane of Caco-2 cells. *Am. J. Physiol. Cell Physiol.* **290**, C1287–C1296 (2006).
35. C. L. Bowman, P. A. Gottlieb, T. M. Suchyna, Y. K. Murphy, F. Sachs, Mechanosensitive ion channels and the peptide inhibitor GsMTx-4: History, properties, mechanisms and pharmacology. *Toxicon* **49**, 249–270 (2007).
36. T. M. Suchyna, J. H. Johnson, K. Hamer, J. F. Leykam, D. A. Gage, H. F. Clemo, C. M. Baumgarten, F. Sachs, Identification of a peptide toxin from *Grammostola spatulata* spider venom that blocks cation-selective stretch-activated channels. *J. Gen. Physiol.* **115**, 583–598 (2000).
37. S. Terryn, F. Jouret, F. Vandenabeele, I. Smolders, M. Moreels, O. Devuyst, P. Steels, E. Van Kerkhove, A primary culture of mouse proximal tubular cells, established on collagen-coated membranes. *Am. J. Physiol. Renal Physiol.* **293**, F476–F485 (2007).
38. A. Luciani, C. Sirac, S. Terryn, V. Javaugue, J. A. Prange, S. Bender, A. Bonaud, M. Cogné, P. Aucouturier, P. Ronco, F. Bridoux, O. Devuyst, Impaired lysosomal function underlies monoclonal light chain-associated renal fanconi syndrome. *J. Am. Soc. Nephrol.* **27**, 2049–2061 (2016).
39. W. Liedtke, J. M. Friedman, Abnormal osmotic regulation in *trpv4*$^{-/-}$ mice. *Proc. Natl. Acad. Sci. U.S.A.* **100**, 13698–13703 (2003).
40. S. Janas, F. Seghers, O. Schakman, M. Alsady, P. Deen, J. Vriens, F. Tissir, B. Nilius, J. Loffing, P. Gailly, O. Devuyst, TRPV4 is associated with central rather than nephrogenic osmoregulation. *Pflugers Arch.* **468**, 1595–1607 (2016).
41. A. Bernard, R. Lauwerys, Low-molecular-weight proteins as markers of organ toxicity with special reference to Clara cell protein. *Toxicol. Lett.* **77**, 145–151 (1995).
42. J. Eckel, P. J. Lavin, E. A. Finch, N. Mukerji, J. Burch, R. Gbadegesin, G. Wu, B. Bowling, A. Byrd, G. Hall, M. Sparks, Z. S. Zhang, A. Homstad, L. Barisoni, L. Birbaumer, P. Rosenberg, M. P. Winn, TRPC6 enhances angiotensin II-induced albuminuria. *J. Am. Soc. Nephrol.* **22**, 526–535 (2011).
43. E. B. Rankin, J. E. Tomaszewski, V. H. Haase, Renal cyst development in mice with conditional inactivation of the von Hippel-Lindau tumor suppressor. *Cancer Res.* **66**, 2576–2583 (2006).
44. R. Kalluri, T. M. Danoff, H. Okada, E. G. Neilson, Susceptibility to anti-glomerular basement membrane disease and Goodpasture syndrome is linked to MHC class II genes and the emergence of T cell-mediated immunity in mice. *J. Clin. Invest.* **100**, 2263–2275 (1997).
45. Y. Sado, A. Boutaud, M. Kagawa, I. Naito, Y. Ninomiya, B. G. Hudson, Induction of anti-GBM nephritis in rats by recombinant α3(IV)NC1 and α4(IV)NC1 of type IV collagen. *Kidney Int.* **53**, 664–671 (1998).
46. C. D. Cox, C. Bae, L. Ziegler, S. Hartley, V. Nikolova-Krstevski, P. R. Rohde, C.-A. Ng, F. Sachs, P. A. Gottlieb, B. Martinac, Removal of the mechanoprotective influence of the cytoskeleton reveals PIEZO1 is gated by bilayer tension. *Nat. Commun.* **7**, 10366 (2016).
47. S. Loukin, X. Zhou, Z. Su, Y. Saimi, C. Kung, Wild-type and brachyolmia-causing mutant TRPV4 channels respond directly to stretch force. *J. Biol. Chem.* **285**, 27176–27181 (2010).
48. R. Köhler, W.-T. Heyken, P. Heinau, R. Schubert, H. Si, M. Kacik, C. Busch, I. Grgic, T. Maier, J. Hoyer, Evidence for a functional role of endothelial transient receptor potential V4 in shear stress-induced vasodilatation. *Arterioscler. Thromb. Vasc. Biol.* **26**, 1495–1502 (2006).
49. B. D. Matthews, C. K. Thodeti, J. D. Tytell, A. Mammoto, D. R. Overby, D. E. Ingber, Ultra-rapid activation of TRPV4 ion channels by mechanical forces applied to cell surface β1 integrins. *Integr. Biol.* **2**, 435–442 (2010).
50. T. Sokabe, T. Fukumi-Tominaga, S. Yonemura, A. Mizuno, M. Tominaga, The TRPV4 channel contributes to intercellular junction formation in keratinocytes. *J. Biol. Chem.* **285**, 18749–18758 (2010).
51. B. Nilius, T. Voets, The puzzle of TRPV4 channelopathies. *EMBO Rep.* **14**, 152–163 (2013).
52. Z. Deng, N. Paknejad, G. Maksaev, M. Sala-Rabanal, C. G. Nichols, R. K. Hite, P. Yuan, Cryo-EM and X-ray structures of TRPV4 reveal insight into ion permeation and gating mechanisms. *Nat. Struct. Mol. Biol.* **25**, 252–260 (2018).
53. Z. Du, Y. Duan, Q. S. Yan, A. M. Weinstein, S. Weinbaum, T. Wang, Mechanosensory function of microvilli of the kidney proximal tubule. *Proc. Natl. Acad. Sci. U.S.A.* **101**, 13068–13073 (2004).
54. Z. Du, Q. Yan, Y. Duan, S. Weinbaum, A. M. Weinstein, T. Wang, Axial flow modulates proximal tubule NHE3 and H-ATPase activities by changing microvillus bending moments. *Am. J. Physiol. Renal Physiol.* **290**, F289–F296 (2006).
55. M. Pohl, Q. Shan, T. Petsch, B. Styp-Rekowska, P. Matthey, M. Bleich, S. Bachmann, F. Theilig, Short-term functional adaptation of aquaporin-1 surface expression in the proximal tubule, a component of glomerulotubular balance. *J. Am. Soc. Nephrol.* **26**, 1269–1278 (2015).
56. V. Raghavan, Y. Rbaibi, N. M. Pastor-Soler, M. D. Carattino, O. A. Weisz, Shear stress-dependent regulation of apical endocytosis in renal proximal tubule cells mediated by primary cilia. *Proc. Natl. Acad. Sci. U.S.A.* **111**, 8506–8511 (2014).
57. M. Delling, A. A. Indzhykulian, X. Liu, Y. Li, T. Xie, D. P. Corey, D. E. Clapham, Primary cilia are not calcium-responsive mechanosensors. *Nature* **531**, 656–660 (2016).
58. M. R. Quinlan, N. G. Docherty, R. W. Watson, J. M. Fitzpatrick, Exploring mechanisms involved in renal tubular sensing of mechanical stretch following ureteric obstruction. *Am. J. Physiol. Renal Physiol.* **295**, F1–F11 (2008).
59. L. D. Alexander, S. Alagarsamy, J. G. Douglas, Cyclic stretch-induced cPLA$_2$ mediates ERK 1/2 signaling in rabbit proximal tubule cells. *Kidney Int.* **65**, 551–563 (2004).
60. E. J. Lewis, X. Xu, Abnormal glomerular permeability characteristics in diabetic nephropathy: Implications for the therapeutic use of low-molecular weight heparin. *Diabetes Care* **31** (Suppl 2), S202–S207 (2008).
61. M. Ludwig, S. K. Sethi, Novel techniques and newer markers for the evaluation of "proximal tubular dysfunction". *Int. Urol. Nephrol.* **43**, 1107–1115 (2011).
62. J. Sun, K. Hultenby, J. Axelsson, J. Nordström, B. He, A. Wernerson, K. Lindström, Proximal tubular expression patterns of megalin and cubilin in proteinuric nephropathies. *Kidney Int. Rep.* **2**, 721–732 (2017).
63. F. Cachat, B. Lange-Sperandio, A. Y. Chang, S. C. Kiley, B. A. Thornhill, M. S. Forbes, R. L. Chevalier, Ureteral obstruction in neonatal mice elicits segment-specific tubular cell responses leading to nephron loss. *Kidney Int.* **63**, 564–575 (2003).
64. R. Rohatgi, D. Flores, Intratubular hydrodynamic forces influence tubulointerstitial fibrosis in the kidney. *Curr. Opin. Nephrol. Hypertens.* **19**, 65–71 (2010).
65. A. T. Wyker, R. C. Ritter, D. n. Marion, J. Y. Gillenwater, Mechanical factors and tissue stresses in chronic hydronephrosis. *Invest. Urol.* **18**, 430–436 (1981).
66. A. Patel, E. Honoré, Polycystins and renovascular mechanosensory transduction. *Nat. Rev. Nephrol.* **6**, 530–538 (2010).
67. T. Gevaert, J. Vriens, A. Segal, W. Everaerts, T. Roskams, K. Talavera, G. Owsianik, W. Liedtke, D. Daelemans, I. Dewachter, F. Van Leuven, T. Voets, D. De Ridder, B. Nilius, Deletion of the transient receptor potential cation channel TRPV4 impairs murine bladder voiding. *J. Clin. Invest.* **117**, 3453–3462 (2007).
68. D. X. Zhang, S. A. Mendoza, A. H. Bubolz, A. Mizuno, Z.-D. Ge, R. Li, D. C. Warltier, M. Suzuki, D. D. Gutterman, Transient receptor potential vanilloid type 4-deficient mice exhibit impaired endothelium-dependent relaxation induced by acetylcholine in vitro and in vivo. *Hypertension* **53**, 532–538 (2009).

Acknowledgments: We thank V. Haase (Vanderbilt University, Nashville) for providing *PEPCK-Cre* mice, and M. de Clippele and R. de Jesus Carvajal Usuga for excellent technical assistance. **Funding:** This work was supported by the Belgian Fund for Scientific Research (FNRS, grants CDR J0080.17 and EQP U.N011.17) and the Concerted Research Action from the General Direction of Scientific Research of the French Community of Belgium (ARC17/22-083) and the Swiss National Science Foundation (project grant 310030_189044). **Author contribution:** R.G., F.S., O.D., and P.G. designed the study, performed experiments, interpreted the data, and wrote the paper. X.Y., O.S., and Y.A. performed experiments and interpreted the data. N.T. and F.T. critically revised the manuscript. All authors provided final approval for the version of the manuscript submitted for publication and agreed to be accountable for the work. **Competing interests:** The authors declare that they have no competing interests. **Data and materials availability:** All data needed to evaluate the conclusions in the paper are present in the paper or the Supplementary Materials. The *PEPCK-Cre* mice require a material transfer agreement from Vanderbilt University.

Submitted 8 May 2020
Accepted 17 September 2020
Published 13 October 2020
10.1126/scisignal.abc6967

Citation: R. Gualdani, F. Seghers, X. Yerna, O. Schakman, N. Tajeddine, Y. Achouri, F. Tissir, O. Devuyst, P. Gailly, Mechanical activation of TRPV4 channels controls albumin reabsorption by proximal tubule cells. *Sci. Signal.* **13**, eabc6967 (2020).

Mechanical activation of TRPV4 channels controls albumin reabsorption by proximal tubule cells

Roberta Gualdani, François Seghers, Xavier Yerna, Olivier Schakman, Nicolas Tajeddine, Younès Achouri, Fadel Tissir, Olivier Devuyst and Philippe Gailly

Sci. Signal. **13** (653), eabc6967.
DOI: 10.1126/scisignal.abc6967

Endocytosis under pressure

The kidneys filter the blood multiple times a day through structures known as glomeruli, and filtered water, solutes, and proteins such as albumin are reabsorbed by the proximal tubule and returned to the circulation. Kidney damage or disease may result in proteinuria, which can lead to nephropathy if left unchecked. Gualdani *et al.* found that mechanosensing induced by fluid flow through the proximal tubule activated the cation channel TRPV4 to promote the endocytosis of albumin in tubular epithelial cells and, thus, its retention. Experimental manipulations that increased the permeability of the glomerular filter exacerbated proteinuria in mice lacking TRPV4 globally or specifically in the proximal tubule. Thus, defects in TRPV4-mediated endocytosis may underlie proteinuria, a common symptom of many kidney diseases.